



## Hyperspectral Mineral Target Detection Based on Density Peak

Yani Hou, Wenzhong Zhu and Erli Wang

School of Computer Science, Sichuan University of Science & Engineering, Zigong, Sichuan, 643000, China

### ABSTRACT

Hyperspectral remote sensing, with its narrow band imaging, provides the potential for fine identification of ground objects, and has unique advantages in mineral detection. However, the image is nonlinear and the pure pixel is scarce, so using standard spectrum detection will lead to an increase of the number of false alarm and missed detection. The density peak algorithm performs well in high-dimensional space and data clustering with irregular category shape. This paper used the density peak clustering to determine the cluster centers of various categories of images, and took it as the target spectrum, and took the clustering results as the ground data. Two methods of HUD and OSP were used to detect the image, and the correlation coefficients of the spectrum of each cluster center and the mineral spectrum of the spectral library were obtained. Finally, the results were compared with the mapping results of Clark et al. The experimental results showed that the cluster center spectrum as the target can well detected the distribution of the corresponding minerals, and it has higher correlation coefficient with mineral in the result of mapping.

**KEYWORDS:** Hyperspectral remote sensing; Density peak; Mineral detection; Correlation coefficient.

### 1 INTRODUCTION

HYPERSPECTRAL remote sensing technology is one of the greatest achievements in the field of remote sensing in 1980s. It obtains many spectral images of ground objects of many continuous bands while observing the earth from the space, achieving the purpose of directly identifying objects on the earth's surface from space, therefore, the hyperspectral remote sensor is commonly called imaging spectrometer. Compared with the traditional multispectral scanner, the imaging spectrometer can get the continuous images of hundreds of bands, and each image pixel can extract a spectral curve (Tong, Zhang, & Zheng, 2006). The characteristics of the union of image and spectrum require people to understand the transformation of ground objects in space dimension from spectral dimension. The processing and analysis of two-dimensional space images need to be converted to the processing and analysis of spectral curves extracted from each pixel (Zhang, 2006).

Mineral mapping can be said to be the most successful application field of the hyperspectral technology, which can also give full play to the advantages of technology. It enables the remote

sensing geology to develop from identifying lithology to identify the chemical composition and crystal structure of single minerals and even minerals (Pieters, & Englert, 1993), which will be one of the important high-tech technologies to support the investigation of strategic mineral resources, environmental monitoring and control and the Project Moonshot in China (Wang, Gan, & Yan, 2010). In the early stage, the study of hyperspectral remote sensing for rock and mineral identification was mainly focused on the response law of reflectance spectrum of rocks and minerals. In the 1970s and 1980s, the researchers measured and analyzed the spectral characteristics of a large number of typical rocks and minerals, including the mixture of montmorillonite and black carbon particles, anhydrous carbonate, silicate minerals, etc (Hunt, 1977, 1979; Clark, 1983; Gafeey, 1987; Li, & Liu, 2008). The measurement and analysis of the spectral characteristics of rocks and minerals have laid a foundation for the rock and mineral identification of hyperspectral remote sensing.

Since 1990s, the research focus has gradually shifted from the characteristics law of spectral response of rock and mineral to hyperspectral remote sensing rock and mineral identification technology, and has formed a series of complete processes of

hyperspectral remote sensing rock and mineral information identification. Typical: a set of methods developed by American AIG company (Kruse, 2003): minimum noise fraction (MNF), pixel purity index (PPI), n-dimensional visualized analysis and spectral angle mapping (SAM) or mixture tuned matched filtering (MTMF), and Tetracorder system developed by USGS and JPL in the United States (Clark, Swayze, & Livo, 2003). The ideas adopted by these methods are as follows: After the preprocessing of atmospheric correction, geometric correction and noise suppression of hyperspectral remote sensing images, the reference spectrum and image pixel spectrum are processed and analyzed, and the categories, composition or abundance of minerals are obtained, thus realizing the accurate identification of rocks and minerals (Zhang, Qin, & Chen, 2015; Lu, 2018; Ye, Meng, & Zhang, 2018).

In this paper, the clustering algorithm is applied to hyperspectral mineral target detection to verify the feasibility taking the clustering center as the target. The structure of this paper is as follows: the second part introduces the density peak clustering algorithm, the third part introduces two target detection algorithms, the fourth part uses hyperspectral images for clustering and detection experiments, and evaluates the experimental results, and the fifth part draws the conclusion.

## 2 DENSITY PEAK CLUSTERING ALGORITHM

At present, clustering methods are still mostly used in image classification field. Classical clustering methods include K-mean clustering, IsoData clustering, Naive Bayes method and so on. (Parastou, Soheil, & Abbas, 2017) In recent years, the density based clustering algorithm has gained the extensive attention from the researchers. The DBSCAN (Li, 2010) method has the function of noise processing. According to whether the density reaches the threshold, the range of data is divided. The DBSCAN algorithm has two advantages: first, the structure is simple and the clustering efficiency is high; second, the aggregation data sets of various shapes can be identified, and the noise interference can be avoided effectively. However, the algorithm also has its own defects. The algorithm must manually set two parameters. These two parameters have great influence on the clustering results and the stability of the algorithm is poor. The other method is OPTICS (Duan, 2013), which is an improved algorithm based on the previous method, which improves the stability of the algorithm. By generating an ordered cluster sequence, the algorithm can get the aggregation of different densities. The difficulty of the algorithm is to maintain the ordered list of the direct reachable points of the core points, and increase the complexity of the algorithm (Lu, 2017).

The essence of the clustering algorithm based on the peak density lies in the determination of the cluster

center. First, the point with the largest density  $\rho_i$  is found, and then the point with the larger distance between the points with the larger density can be identified as the cluster center.

The two important parameters  $\rho_i$  and  $\delta_i$  of the sample points are defined as follows (Rodriguez, & Laio, 2014):

$$\rho_i = \sum_j \chi(d_{ij} - d_c)$$

$$\text{Among them, } \chi(x) = \begin{cases} 1, & x \leq 0 \\ 0, & x > 0 \end{cases}$$

$d_{ij}$  represents the distance between the sample point  $i$  and the sample point  $j$ , and  $d_c$  represents the truncation distance, that is the threshold of distance.

$\rho_i$  represents the number of sample points in a circular region with  $i$  as the center of the sample point and  $d_c$  as the radius. The larger the  $\rho_i$ , the more points around the sample point  $i$  less than the distance of  $d_c$  from  $i$ , which means that the points around  $i$  are thicker.

$$\delta_i \text{ is defined as: } \delta_i = \min_{j: \rho_j > \rho_i} (d_{ij})$$

$\delta_i$  represents the minimum distance between the sample point  $i$  and the sample point whose density is greater than  $i$ , and  $\delta_i$  describes the difference among categories. The larger the  $\delta_i$ , the larger the distance between the sample point  $i$  and the sample point whose density is greater than it, indicating that this point is not the same class as the point of greater density.

The goal of clustering is that the smaller the difference, the better in the same category, and the higher the difference between categories, the better. It can be seen from the above two parameters that the larger the  $\rho_i$ , the larger the density of the sample point, and the more points around it, and the larger the probability of the sample point as the cluster center, and the points around it should be clearly divided into the same category. Under the premise of satisfying this condition, we should also consider that the larger the gap between the classes, the better. And the larger the  $\delta_i$ , the larger the difference between classes.

According to the above discussion, we only need to find the point with larger  $\rho_i$  and  $\delta_i$ , and then we can determine the cluster center. When we calculate the values of  $\rho_i$  and  $\delta_i$  of the sample point, we can characterize the sample point into decision diagrams, and then the decision diagram is used to intuitively

determine the cluster center. After determining the cluster center, we need to classify other sample points. The basis of distribution is that the attribution of a sample point is consistent with the attribution of the nearest point whose density is higher than it.

Due to the uniqueness of the clustering algorithm classification criteria of density peaks, it can identify all kinds of data classes of different shapes.

### 3 TARGET DETECTION METHOD

HYPERSPETRAL target detection methods are classified according to different criteria. According to the target pixel size, it can be divided into pure pixel target detection method and a sub-pixel target detection method. According to whether the target spectrum is a prior knowledge, it can be divided into the target matching detection method and the abnormal target detection method. According to the different algorithms, it can be divided into the method based on hypothesis testing and the method based on projection. Classical detection methods have matured and new algorithms have emerged one after another. This section introduces two classical target detection algorithms.

#### 3.1 HUD Algorithm

HUD (hybrid unstructured detector) (Du, 2010) is evolved from ACE, and ACE is a very effective sub-pixel target detection method. Specifically, the background structure is completely removed in the ACE method, and the background is assumed to be a Gaussian distribution with zero mean and covariance of  $\sigma^2\Gamma$ .

ACE can be expressed as:

$$D_{ACE}(\mathbf{r}) = \frac{\mathbf{r}^T \Gamma^{-1} \mathbf{D} (\mathbf{D}^T \Gamma^{-1} \mathbf{D})^{-1} \mathbf{D}^T \Gamma^{-1} \mathbf{r}}{\mathbf{r}^T \Gamma^{-1} \mathbf{r}}$$

$\mathbf{r}$  is a spectral vector of a pixel in a hyperspectral image,  $\mathbf{D}$  is the target spectral matrix, and  $\Gamma$  is the background covariance matrix.

The HUD algorithm  $(\mathbf{D}^T \Gamma^{-1} \mathbf{D})^{-1} \mathbf{D}^T \Gamma^{-1} \mathbf{r}$  will be replaced by the real spectral component  $\hat{\mathbf{a}}_{FCLS}$  obtained by the full constraint least square spectral decomposition, that is:

$$D_{HUD}(\mathbf{r}) = \frac{\mathbf{r}^T \Gamma^{-1} \mathbf{D} \hat{\mathbf{a}}_{FCLS}}{\mathbf{r}^T \Gamma^{-1} \mathbf{r}}$$

$\hat{\mathbf{a}}_{FCLS}$  can be calculated by

$$\min_a (\mathbf{x} - \mathbf{E}a)^T \Gamma^{-1} (\mathbf{x} - \mathbf{E}a), \quad a_i \geq 0$$

Among them,  $\mathbf{x}$  represents the pixel spectrum,  $\mathbf{E}$  represents the end-member matrix, and  $a$  represents the abundance.

#### 3.2 OSP Algorithm

The idea of orthogonal subspace projection (OSP) algorithm is to maximize the signal-to-noise ratio of background orthotopic subspace projection (Huang, 2014; Hou, 2016). Assuming that there is only one kind of target to be detected in hyperspectral data  $\mathbf{X}$ , the signal to be detected is set as  $\mathbf{t}$ , and its abundance is  $a\mathbf{t}$ . The background signal is set as  $\mathbf{U}$ , and the percentage of the background is  $a\mathbf{U}$ , so there is:

$$\mathbf{X} = \mathbf{t}\alpha_t + \mathbf{U}\alpha_U + \varepsilon$$

The OSP algorithm gives the projection operator  $P_U^\perp$  to remove the unused background  $\mathbf{U}$ , and  $P_U^\perp$  is defined as:

$$P_U^\perp = \mathbf{I} - \mathbf{U}\mathbf{U}^\#$$

$\mathbf{U}^\#$  is called the pseudo inverse of  $\mathbf{U}$ ,  $\mathbf{U}^\# = (\mathbf{U}^T \mathbf{U})^{-1} \mathbf{U}^T$ . The function of the projection operator  $P_U^\perp$  is to project the hyperspectral data into the subspace spanned by the background. The formula is as follows:

$$P_U^\perp \mathbf{X} = P_U^\perp \mathbf{t}\alpha_t + P_U^\perp \mathbf{U}\alpha_U + P_U^\perp \varepsilon = P_U^\perp \mathbf{t}\alpha_t + P_U^\perp \varepsilon$$

At this point, the background signal  $\mathbf{U}$  is eliminated. Then, we look for a vector  $\mathbf{w}$  to maximize the signal to noise ratio (SNR) of the output  $\mathbf{w} P_U^\perp \mathbf{X}$ .

$$SNR(\mathbf{w}) = \frac{(\mathbf{w}^T P_U^\perp \mathbf{t}) \alpha_t^2 (\mathbf{t}^T P_U^\perp \mathbf{w})}{\mathbf{w}^T P_U^\perp E[\varepsilon \varepsilon^T] P_U^\perp \mathbf{w}}$$

The solution of the upper form is equivalent to solving one eigenvalue problem.

$$(P_U^\perp)^{-1} P_U^\perp \mathbf{t} \mathbf{t}^T (P_U^\perp)^T \mathbf{w} = \lambda \mathbf{w}$$

$\mathbf{w} = \kappa \mathbf{t}$  is obtained, among which  $\kappa$  is a integer. Therefore, the OSP operator is finally in the form of:

$$q^T = \mathbf{t}^T P_U^\perp$$

The OSP algorithm can eliminate the background influence and suppress the noise signal while retaining the target signal to the maximum extent (Wang, 2014).

## 4 EXPERIMENT AND ANALYSIS

### 4.1 Experimental Data

THIS experiment used the AVIRIS (Airborne Visible Infrared Imaging Spectrometer) hyperspectral data of Cuprite copper mine area of Nevada in America, and combined with the spectral library of geological survey in the United States (usgs\_min.sli). AVIRIS can provide a whisk broom imaging with spectral resolution of 10 nm, ground pixel resolution

of 20 m, and spectral range of 0.2~2.4  $\mu\text{m}$  (Wang et al,2010).

The Cuprite mining area is divided into east and west two north-south elongated alteration zones by road No.95. There are mainly outcrop rocks in the eastern region, including tertiary volcanic rocks and quaternary alluvial rocks, while there are cambrian metamorphic sedimentary rock, tertiary volcanic rocks and quaternary alluvial rocks. The experimental area has been an important experimental area for geological research since the 1970s due to its good rock outcrop, diversified mineral assemblage, dry climate and convenient transportation.

This experiment selected a part of the region, and the size was 60\*60. In addition to the water vapor absorption and low signal to noise ratio band, there were 202 remaining bands. The study area image is shown in Figure 1. Figure 2 shows the mapping results of Clark and Swayze (Clark, &Swayze,2003) in the corresponding region, which contains Na82 Alunite, Kaolinite, high-Al muscovite and other minerals and also a mixture of several types of minerals.

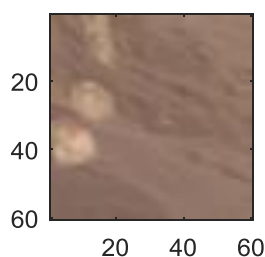


Figure 1. Cuprite research area

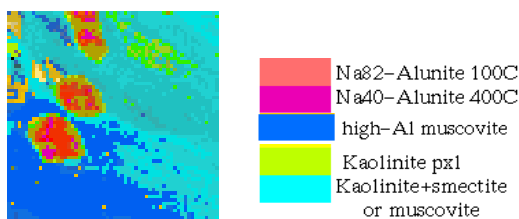


Figure 2. The mapping results by Clark et al

#### 4.2 Experimental Method

In this experiment, the SAM (Spectral Angle Mapper) method was first used to obtain the spectral angle between pixels in the image. The spectral angle matching technique is a measure based on the similarity of spectral dimension curves. It determines the similarity between them by calculating the angle between the spectral vectors. The smaller the angle, the greater the similarity between the two (Wang et al, 2010). The spectral angle was used as the raw data of the density peak clustering algorithm, and the local density and the local minimum distance were calculated to make the decision diagram.

Secondly, according to the principle of density peak clustering, some isolated points were manually

selected as cluster centers from the decision diagram, and then the number of cluster centers and the array of attribution markers were initialized, and the clustering results were obtained after statistical classification.

Thirdly, according to the location of the cluster center, the location spectrum was extracted from the image, which was used as the target spectrum. The attribution marker array was used as ground data in clustering results, HUD and OSP algorithms were used to detect, and the detection rate, false alarm rate, ROC curve and other indexes were used to evaluate the results.

The American geological exploration spectrum library (usgs\_min.sli) can be obtained from the ENVI. Finally, the correlation coefficient between the standard mineral spectrum and the cluster center spectrum was obtained. The correlation coefficient solution formula is as follows:

$$CC = \frac{\langle s_o, s_e \rangle}{\sqrt{\langle s_o, s_o \rangle \langle s_e, s_e \rangle}}$$

The experimental flow chart is shown in Figure 3.

## 4.2 Experimental Results

### 4.2.1 Cluster Results

By calculating the local density and local minimum distance, the decision graph and two-dimensional data distribution graph are shown in Figure 4. In the decision graph, the abscissa represents the local density, the ordinate represents the local minimum distance, and the color points in the coordinate are the isolated points selected by the manual frame, which are also the five cluster centers of the experiment. The cluster results are shown in Figure 5.

Table 1 shows the location of five cluster centers and the number of elements contained in each category, so as to provide a standard for subsequent detection and evaluation.

### 4.2.2 Target Detection Results

The spectral curves of the five cluster centers are shown in Figure 6, and they are used as the target spectrum. The HUD and OSP methods are used to detect the target in the image. The detection result graphs are shown in Figure 7, and the ROC curve is shown in Figure 8.

By calculating the local density and local minimum distance, the decision graph and two-dimensional data distribution graph are shown in Figure 4. In the decision graph, the abscissa represents the local density, the ordinate represents the local minimum distance, and the color points in the coordinate are the isolated points selected by the manual frame, which are also the five cluster centers of the experiment. The cluster results are shown in Figure 5.

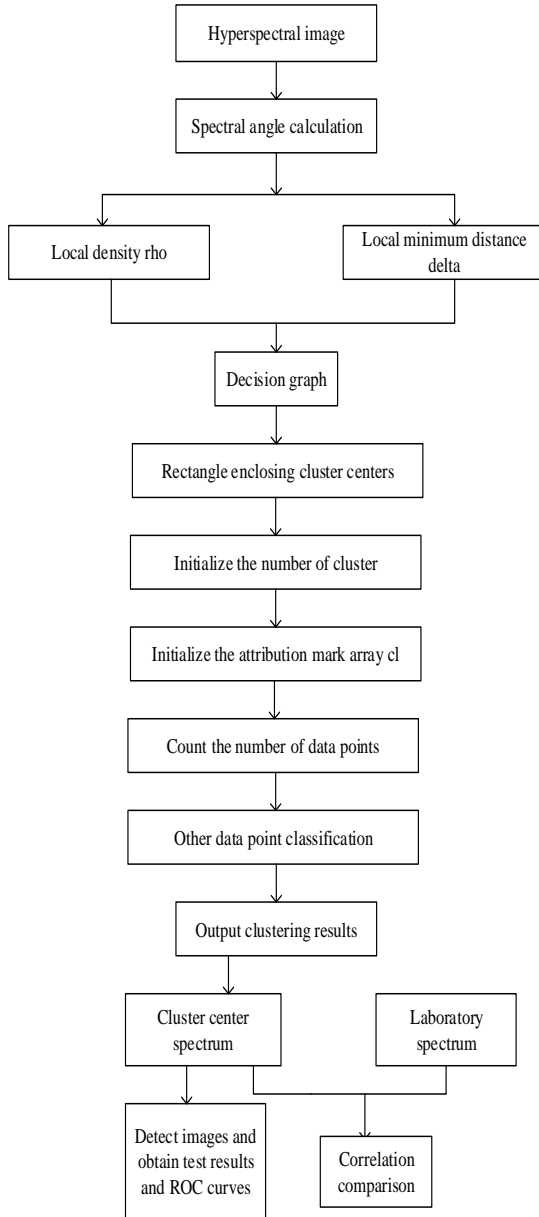


Figure 3. Experimental flow chart

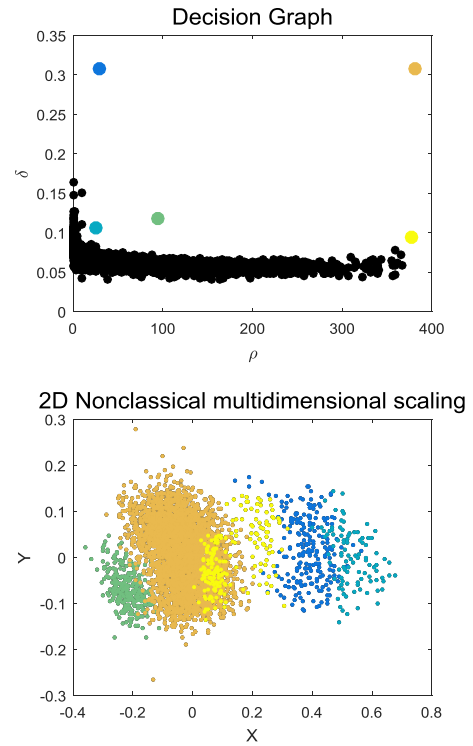


Figure 4. Decision graph and two-dimensional data distribution graph

Table 1 Cluster center coordinates and the number of various elements

Category	Central position	Element number
1	(5,13)	215
2	(27,13)	98
3	(57,26)	286
4	(8,36)	2806
5	(41,51)	195

Table 1 shows the location of five cluster centers and the number of elements contained in each category, so as to provide a standard for subsequent detection and evaluation.

#### 4.3.2 Target Detection Results

The spectral curves of the five cluster centers are shown in Figure 6, and they are used as the target spectrum. The HUD and OSP methods are used to detect the target in the image. The detection result graphs are shown in Figure 7, and the ROC curve is shown in Figure 8.

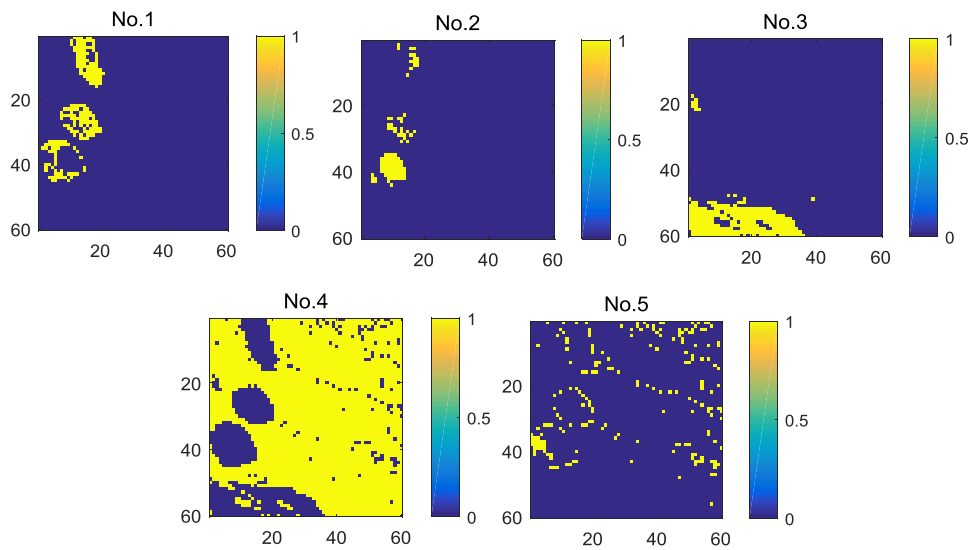


Figure 5. Clustering result graph

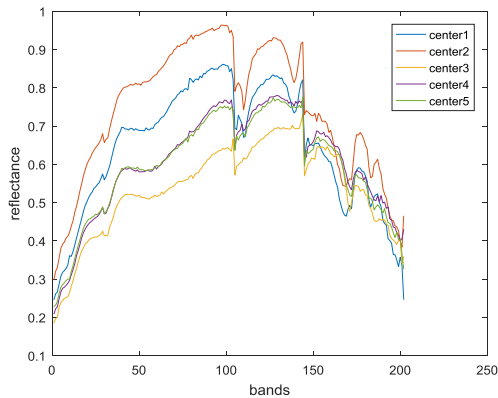


Figure 6. Cluster center spectral curve

Figure 7 (a) - (e) shows the detection results of 5 kinds of targets. Compared with Figure 5, it can be seen that both HUD and OSP two algorithms can detect the target in the image, however, in the first, second, fifth class of detection results, HUD produces less false alarm, and in the third, fourth detection results, the OSP produces less false alarm. It can be seen from the ROC curve in Figure 8 that the two algorithms show better performance. Table 2 and 3 show the false alarm rate, detection rate and missed alarm rate of the two methods. The threshold is set to 0.01, and the missed alarm rate and false alarm rate are calculated. At the same time, the false alarm rate is counted when the detection rate is 0.5.

From Table 2 and 3, we can find that the HUD and OSP methods can show high detection rate and low false alarm rate under a specific threshold. In the second class detection results, the false alarm rate of

the HUD method is only 0.05 when the detection rate is 0.85, and in the fourth class detection result, the detection rate is 1 when the false alarm rate of the OSP method is 0.2. When the detection rate is 0.5, HUD and OSP methods both maintain low false alarm rate, and the HUD false alarm rate is all below 0.15.

#### 4.3.3 Correlation Coefficient between Mineral and Cluster Center

Combined with the US geological exploration spectrum library (usgs\_min.sli), we obtained the correlation coefficients between the five cluster center spectra and 481 spectra in the spectral library. The one with high correlation coefficient was chosen as the corresponding mineral. The selection results are shown in Table 4.

As can be seen from Table 4, the first class corresponds to Na<sub>8</sub>2 Alunite, the second class corresponds to the Na<sub>0</sub>3 Alunite, the third class corresponds to the High Al Muscovite GDS107, the fourth class corresponds to the Kaolinite, and the fifth class corresponds to the Kaolinite pxl. However, the correlation coefficient between the fourth class and Kaolinitepxl is 0.69, which may be in a mixed state of Kaolinite and other minerals. According to the mapping results of Clark et al in Figure 2, there is no Na<sub>4</sub>0 Alunite spectrum in the spectral library, so they choose Na<sub>0</sub>3 Alunite which is similar to it, and the minerals corresponding to the high correlation coefficient are more accurate.

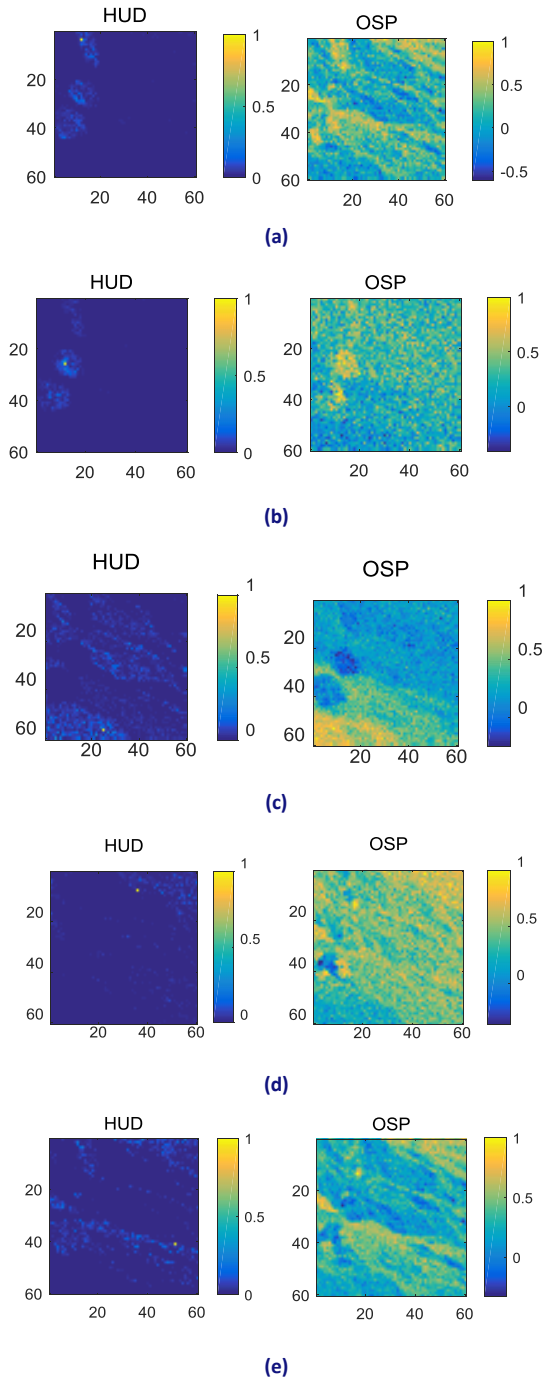


Figure 7. Detection results (a) category I,(b) category II,(c) category III, (d) category IV,(e) category V

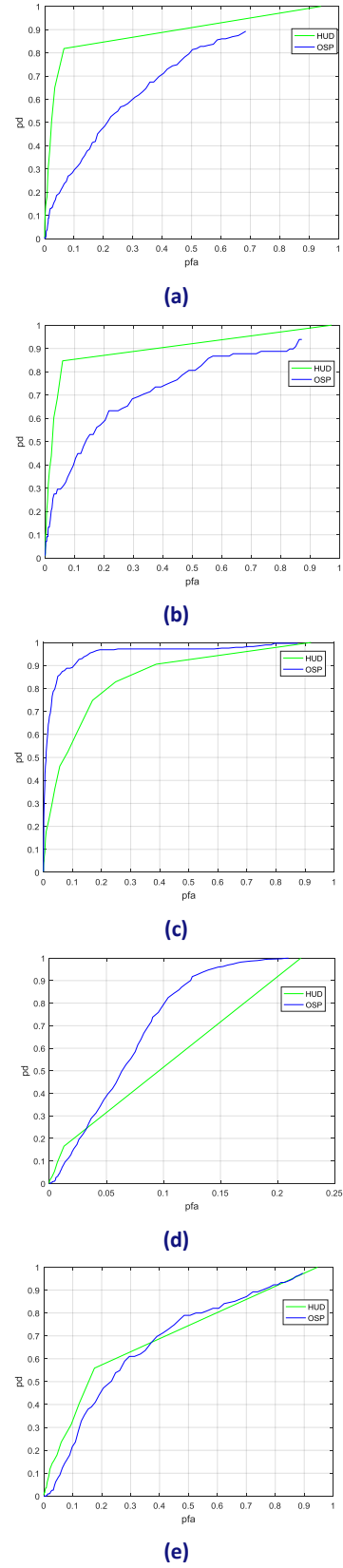


Figure 8. ROC curves of detection results (a) category I,(b) category II,(c) category III,(d) category IV,(e) category V

**Table 2** Detection rate, false alarm rate and missed alarm rate of HUD detection results

Class	Threshold	Pfa	Pd	Missed Alarm Number	Missed Alarm Rate	Pfa ( pd=0.5)
Center1	0.01	<b>0.06</b>	<b>0.83</b>	38	<b>0.17</b>	<b>0.02</b>
Center2	0.01	<b>0.05</b>	<b>0.85</b>	15	<b>0.15</b>	<b>0.02</b>
Center3	0.01	<b>0.39</b>	<b>0.91</b>	27	<b>0.09</b>	<b>0.02</b>
Center4	0.01	<b>0.01</b>	<b>0.17</b>	2339	<b>0.83</b>	<b>0.09</b>
Center5	0.01	<b>0.17</b>	<b>0.56</b>	86	<b>0.44</b>	<b>0.15</b>

**Table 3** Detection rate, false alarm rate and missed alarm rate of OSP detection results

Class	Threshold	Pfa	Pd	Missed Alarm Number	Missed Alarm Rate	Pfa ( pd=0.5)
Center1	0.01	<b>0.67</b>	<b>0.89</b>	25	<b>0.11</b>	<b>0.21</b>
Center2	0.01	<b>0.86</b>	<b>0.94</b>	6	<b>0.06</b>	<b>0.13</b>
Center3	0.01	<b>0.79</b>	<b>0.997</b>	1	<b>0.003</b>	<b>0.008</b>
Center4	0.01	<b>0.2</b>	<b>0.9993</b>	2	<b>0.0007</b>	<b>0.06</b>
Center5	0.01	<b>0.88</b>	<b>0.97</b>	6	<b>0.03</b>	<b>0.22</b>

**Table 4** Selection of spectral correlation coefficient between clustering center and spectral library

CC	Na82 Alunite	Na03 Alunite	High- Al Muscovite GDS107	Kaolinite	Kaolinite pxl
Center1	0.7328	0.5797	0.3754	0.5531	0.2964
Center2	0.5957	0.7134	0.3229	0.4810	0.5637
Center3	0.2432	0.1618	0.9097	0.4810	0.0557
Center4	0.3653	0.2666	0.3937	0.8332	0.6975
Center5	0.4182	0.4896	0.4531	0.6027	0.8160

## 5 CONCLUSIONS

HYPERSPECTRAL, because of its own characteristics, has significant advantages in the field of target detection, which can solve the problems that the traditional panchromatic images and multispectral images cannot solve. However, the mixed pixel in the image exists widely, which makes the research of the related applications more difficult. The density peak algorithm is based on high-dimensional data, and has the good effect in the data set with uneven density distribution. In this paper, the density peak algorithm is used to cluster the images, determine the cluster centers of all kinds of images and take them as the target spectrum. The clustering results are used as the ground data, and the two methods of HUD and OSP are used to detect the images, and the correlation coefficients of the spectrum of each cluster center and the spectral library mineral spectra are obtained. Finally, the result is compared with the mapping results of Clark et al. The experimental results show that the cluster center spectrum as the target can detect the location of the corresponding mineral target in the image, which has high detection rate and low false alarm rate, and has higher correlation coefficient with mineral in the result of mapping, indicating that the cluster center in the image is similar to pure pixel. However, in the process of clustering, manual selection of cluster centers can not automate the algorithm, the small targets in sub-pixel can not be

detected well, and the memory and time consumption in large size images research are higher. Therefore, the optimization of the algorithm and the improvement of efficiency have become a problem to be solved in the future.

## 6 DECLARATIONS

ETHICAL approval and consent to participate: Approved.

Consent for publication: Approved.

Availability of supporting data: Approved.

## 7 COMPETING INTERESTS

THERE no potential competing interests in our paper. And all authors have seen the manuscript and approved to submit to your journal. We confirm that the content of the manuscript has not been published or submitted for publication elsewhere.

## 8 FUNDING:

This work is supported by:

1. Sichuan science and Technology Department (2017GZ0303 and 2018GZ0243)
2. Zigong science and Technology Bureau (2016DZ11)
3. Sichuan provincial academician (expert) workstation (2015YSGZZ01 and 2015YSGZZ04)

4. Key Laboratory Higher Education of Sichuan Province for Enterprise Informationalization and IOT (2016WYY01 and 2017WYY01);

5. Sichuan Key Provincial Research Base of Intelligent Tourism (ZHY17-02 and ZHYJ18-01)

## 9 AUTHORS' CONTRIBUTIONS

ALL authors take part in the discussion of the work described in this paper. The author Wang Erli wrote the first part of the paper. The author Hou ya'ni did all experiments of the paper and wrote the rest of the paper, Zhu Wenzhong revised the paper in different version of the paper, respectively.

1. Our work is to apply the peak density clustering method to hyperspectral mineral target detection. Our method does not have any prior knowledge of images (for example, known types of minerals in an image). It only uses clustering methods to identify clustering centers for mineral detection, to evaluate detection results, and using correlation coefficients to search corresponding minerals from the USGS spectral library.

2. The novelty of our method is that the cluster center is used as pure pixel to optimize the detection effect and to determine the mineral species.

## 10 REFERENCES

- Clark, R.N.(1983). Spectral properties of mixture of montmorillonite and dark carbon grains: Implications for remote sensing minerals containing chemically and physically absorbed water. *Geophysical Research Journal*, 88, 10635-10644.
- Clark, R. N., Swayze, G. A., & Livo, K. E. (2003). Imaging spectroscopy: Earth and planetary remote sensing with the USGS Tetracorder and expert systems. *Geophysical Research Journal*, 108 (12), 5131-5144.
- Du, B. (2010). Sub-Pixel Target Detection from Hyperspectral Remote Sensing Imagery (Doctoral dissertation). Retrieved from CNKI.
- Duan, M.X. & Tang, C.L. (2013). Realization of Clustering Algorithm Based on Density. *Journal of Jishou University (Natural Science Edition)*, 34(1), 26-27.
- Gafeey, S.J. (1987). Spectral reflectance of carbonate minerals in the visible and near infrared (0.35-2.55 microns): anhydrous carbonate minerals. *Geophysical Research Journal*, 98, 1429-1440.
- Hou, Y.N. (2016). *Research on Mineral Spectral Feature Blind Extraction and Target Detection in hyperspectral Image* (Master's thesis). Available from CNKI.
- Huang, Z.H. (2014). *A Study of Hyperspectral Subpixel Target Detection* (Master's thesis). Available from CNKI.
- Hunt, G.R. (1977). Spectral signatures of particulate minerals in visible and near IR. *Geophysics*, 42(3), 501-503.
- Hunt, G.R.(1979). Near-infrared (1.3-2.4  $\mu$ m) spectral of alteration minerals-potential for use in remote-sensing. *Geophysics*, 44 (12), 1974-1986.
- Kruse, F. A. (2003, June). *Preliminary results-hyperspectral mapping of coral reef systems using EO-1 Hyperion Buck Island and U.S. Virgin Islands. Proceedings of the 12th JPL Airbone Geoscience Workshop*, Pasadena, California, USA: JPL publication.
- Li, X. W., & Liu, S.H. (2008) *Principle and Application of Remote Sensing*. Beijing: Science Press. (in Chinese)
- Li W.X. (2010). *Research on Density Based Clustering Algorithm* (Master's thesis). Available from CNKI.
- Lu, H. (2017). *Cluster Algorithm Based on Density Peaks for Hyperspectral Image Classification* (Master's thesis). Available from CNKI.
- Lu, Y. (2018). *Applications of Hyperspectral Mineral Mapping in Mineral and Petroleum Exploration* (Doctoral dissertation). Retrieved from CNKI.
- Parastou. S. E., Soheil S. & Abbas. S (2017). Multi-Objective Complete Fuzzy Clustering Approach. *Intelligent Automation & Soft Computing*, 23, 285-294.
- Pieters, C. M., & Englert, P. A. (1993). *Remote Geochemical Analysis: Elemental and Mineralogical Composition*. USA: Cambridge University Press.
- Rodriguez, A., & Laio, A. (2014). Machine learning. Clustering by fast search and find of density peaks. *Science*, 344(6191), 1492-1496.
- Tong, Q.X., Zhang, B., & Zheng, L.F. (2006). *Hyperspectral Remote Sensing—Principle, Technology and Application*. Beijing: Higher Education Press.
- Wang, J. (2014). *Research on Target Detection and Recognition Based on Hyperspectral Imagery* (Master's thesis). Available from CNKI.
- Wang, R.S., Gan, F.P., & Yan, B.K.(2010). Hyperspectral Mineral Mapping and Its Application. *Remote Sensing for Land and Resources*, 83, 1-13.
- Ye, F.W., Meng, S., & Zhang, C. (2018). Minerageny Study of High-Al, Medium-Al and Low-Al Sericites Identified by Airborne Hyperspectral Remote Sensing Technology. *Acta Geologica Sinica*, 92(02), 395-412.
- Zhang, B. (2002). *Hyperspectral Data Mining Supported by Temporal and Spatial Information* (Doctoral dissertation). Retrieved from CNKI.
- Zhang, C.Y., Qin, Q.M., & Chen. L. (2015). Research and Development of Mineral Identification Utilizing Hyperspectral Remote Sensing. *Optics and Precision Engineering*, 23(8), 2407-2418.

## 11 NOTES ON CONTRIBUTORS



**Yani Hou**, received the master degree in Surveying and Mapping from the University of Electronic Science and Technology of China (UESTC), Chengdu, China, in 2016.

Currently, she is a Teaching Assistant of computer science and technology, Sichuan University of Science &

Engineering. Her research interests include remote sensing, hyperspectral image processing and IOT.

Email: boxcy@163.com



**Wenzhong Zhu**, received the master degree in Computer Science and Technology of Chongqing University of China, Chongqing, China, in 2007.

Currently, he is a Professor of computer science and technology, Sichuan University of Science & Engineering. His research interests include IOT,

cloud computing and intelligent tourism.

Email: zwz@suse.edu.cn



**Erli Wang**, received the master degree in Photogrammetry and remote sensing from Wuhan University, Wuhan, China, in 2015.

Currently, she is a Research Assistant of computer science and technology, Sichuan University of Science & Engineering. Her research

interests include remote sensing, GIS and IOT.

Email: welsuse@suse.edu.cn